2014

X-ray Diffraction Spectroscopy Studies of CuIn2n+1S3n+2 Thin Films

B. Khalfallah
Laboratoire de Photovolta¨ıque et Matriaux Semi-conducteurs - ENIT - Universit Tunis ElManar, BP 37, Le belv´ed`ere 1002-, Tunis, bilel_khalfallah@yahoo.com

N. Khemiri
Laboratoire de Photovolta¨ıque et Matriaux Semi-conducteurs - ENIT - Universit Tunis ElManar, BP 37, Le belv´ed`ere 1002-, Tunis, bilel_khalfallah@yahoo.com

D. Abdelkader
Laboratoire de Photovolta¨ıque et Matriaux Semi-conducteurs - ENIT - Universit Tunis ElManar, BP 37, Le belv´ed`ere 1002-, Tunis, bilel_khalfallah@yahoo.com

M. Kanzari
Laboratoire de Photovolta¨ıque et Matriaux Semi-conducteurs - ENIT - Universit Tunis ElManar, BP 37, Le belv´ed`ere 1002-, Tunis, bilel_khalfallah@yahoo.com

X-ray Diffraction Spectroscopy Studies of $CuIn_{2n+1}S_{3n+2}$ Thin Films

N. Khemiri, B. Khalfallah, D. Abdelkader and M. Kanzari*

Laboratoire de Photovoltaïque et Matriaux Semi-conducteurs - ENIT - Universit Tunis ElManar, BP 37, Le belvédère 1002-, Tunis

Abstract: $CuIn_{2n+1}S_{3n+2}$ (where n = 0, 1, 2, 3 and 5) thin films were deposited at different substrate temperatures (30, 75, 100, 150 and 200 °C) by vacuum evaporation. The films were characterized for their structural properties by using X-ray diffraction (XRD). From the XRD data, we calculated the grain size, the lattice strain, the lattice parameters and the dislocation density for the preferential orientation of $CuIn_{2n+1}S_{3n+2}$ thin films. The effect of the substrate temperature on the structural crystalline quality of the films was also investigated.

Keywords: Thin films, $CuIn_{2n+1}S_{3n+2}$, Vacuum evaporation, Structural properties, Substrate temperature.

1 Introduction

The ternary compound $CuInS_2$ has attracted attention as a promising material for photovoltaic applications, due to its optimum direct band gap of 1.5 eV and its high absorption coefficient. He also contains non-toxic constituents making it suitable for green processing in solar cell fabrication [1,2] . The efficiency of the solar cells made with the two-step electrodeposition and rapid thermal processing RTP low-cost process reaches 11 % by Broussillou et *al*. in 2011 [3] and it rose to 12.8 % by Klenk et *al*. [4]. $CuInS_2$ belongs to the $I - III_{2n+1} - VI_{3n+2}$ ternary materials which are receiving a great deal of attention as candidate materials for visible-light and IR emitters, high-efficiency solar cells, and other semiconductor and quantum-electronic devices [5]. Rud et *al*. [6] studied $CuIn_{2n+1}Se_{3n+2}$ semiconductors with the composition index n = 3, 5 and 6, they found that the weak dependence of the parameters of the bands spectrum and unit cell of these semiconductors at n $\geq$ 2 was attributed to the features of the interatomic interaction in such phases. It was concluded that $CuIn_{2n+1}Se_{3n+2}$ semiconductors can be used in broadband photoconverters of optical radiations. Only few research papers described the preparation and the characterization of $CuIn_{2n+1}S_{3n+2}$ films where n $\geq$ 1, out of which, most of the literature deals with $CuInS_2$ (n = 0) films fabricated by physical or chemical deposition techniques [7,8,9,10]. The formation of $CuIn_{2n+1}S_{3n+2}$

compounds is due to the ordering of the neutral defect pairs $(2V_{Cu^{-1}} + In_{Cu^{2+}})$ and $(2Cu_{In^{-2}} + In_{Cu^{2+}})$ in the $CuInS_2$ phase and this is due to its huge tolerance to off-stoichiometry. [11]. Several studies on structural properties of the $Cu - III_{2n+1} - VI_{3n+2}$ materials have been reported [12,13,14,15,16], where growth conditions and thermal treatment affected the structural properties of the films.In the present study, we have investigated the effect the substrate temperature on the structural properties of thermally evaporated $CuIn_{2n+1}S_{3n+2}$ thin films through their XRD spectra and effect.

2 $CuIn_{2n+1}S_{3n+2}$ materials

$CuIn_{2n+1}S_{3n+2}$ materials are some of the indium-rich compounds, which exist on the pseudo-binary tie line of the Cu_2S - In_2S_3 system. In-rich films with a sulfur deficiency are dominated by both antisite (In on Cu site) donor defects and S vacancies (also donors), yielding highly conductive n-type layers [17]. We have shown in a previous paper [18] that the peak due to the (112) plane has the highest intensity for the $CuInS_2$ and $CuIn_3S_5$ powders while the highest intensity for $CuIn_5S_8$, $CuIn_7S_{11}$ and $CuIn_{11}S_{17}$ powders is the peak due to the (311) plane. The EDX analysis confirmed the chemical composition of the powders. X-ray diffraction (XRD) showed a tetragonal chalcopyrite type structure for $CuInS_2$ and $CuIn_3S_5$ powders with space group $I - 42d$

* Corresponding author e-mail: bilel_khalfallah@yahoo.com

and $P-42c$, respectively. The structure of $CuIn_5S_8$, $CuIn_7S_{11}$ and $CuIn_{11}S_{17}$ powders was cubic spinel (space group $Fd3m$) [13]. This transition in the crystal structure between n = 0 and 1 and n = 2, 3 and 5 in the $CuIn_{2n+1}S_{3n+2}$ system can be explained by the migration of a part of In^{3+} ions towards octahedral sites when the indium atoms increase in the structure. Indeed, the In^{3+} ions can be stabilized in both tetrahedral and octahedral sites but tend to form bonding with octahedral coordinations and as result the crystal structure changes from tetragonal to cubic structure [18].

3 Experiment Work

$CuIn_{2n+1}S_{3n+2}$ thin films were prepared by thermal evaporation of crushed powders from a Tungsten boat on heated and non-heated glass substrates of rectangular shape $(2.5 \times 1.5 cm^2)$ under vacuum (10^{-6} mbar) using a high vacuum coating unit Alcatel. The substrates were placed directly above the source at a distance of 15 cm and were heated by an insulator heater system. The substrate temperature T_s was measured using a thermocouple embedded in the substrate holder underneath the substrates. The glass substrates were previously cleaned with washing agents (commercial detergent, acetone, ethanol and deionized water) before being introduced into the vacuum system. The base pressure of the vacuum system was kept between 10^{-5} and 10^{-6} mbar. The crystalline phase and crystal orientation of the films were examined using a PANalytical X'Pert X-ray diffractometer with monochromatic CuK_a radiation (λ = 0.154056 nm and 40 kV, 30 mA).

4 Results and Discussions

There is an agreement between authors that the increase in the substrate temperature improves the crystallinity of thin films and causes the transition from amorphous to polycrystalline structure [14,15,16]. X-ray diffraction (XRD) is the suitable tool to reveal the changes in the structural properties of thin films. For polycrystalline films, the variations of the intensity of the peaks and their width at half maximum (FWHM) with substrate temperature are evidences on the changes in grain size and lattice strain. The decrease in FWHM means that the grain size had increased. The shifts of the positions of the peaks refer to the changes in the lattice spacing and the lattice parameters. The appearance of some lines and disappearance of others with substrate temperature may mean a phase transition and / or the appearance or disappearance of other phases of the compounds under study or the presence of some elements. In the present work, different experimental results will be discussed to show the effects of the substrate temperature on the

structural properties of $CuIn_{2n+1}S_{3n+2}$ thin films. XRD patterns (10 ° $\leq 2\theta \leq$ 60 °) of $CuIn_{2n+1}S_{3n+2}$ (where n = 0, 1, 2, 3, and 5) films deposited at different substrate temperatures (T_s = 30, 75, 100, 150 and 200 °C) are given in Fig. **1**. It is clear that the films of all compounds deposited on non heated substrate (T_s = 30 °C) are amorphous in nature. As the substrate temperature increases, the films start to become polycrystalline with a preferred orientation along the (112) plane, characteristic of chalcopyrite, structure for $CuInS_2$ and $CuIn_3S_5$ films and the (311) plane, characteristic of cubic spinel structure, for $CuIn_5S_8$, $CuIn_7S_{11}$ and $CuIn_{11}S_{17}$ films. XRD patterns of $CuIn_3S_5$, $CuIn_5S_8$, $CuIn_7S_{11}$ and $CuIn_{11}S_{17}$ films depicts that peaks appear at T_s = 75 °C. However, $CuInS_2$ films become polycristalline at T_s = 100 °C and we note, for $CuInS_2$ film deposited at 150 °C, the apparition of weak reflections related to (103), (004), (200) and (204). At T_s = 200 °C, these peaks disappear and new peaks related to (213), (312) and (224) appear. For $CuIn_7S_{11}$ films formed at 150 and 200 °C, two additional peaks related to (400) and (440) reflections are clearly observed. The substrate temperature plays a key role on the enhancement of crystal quality and on the preferential orientation of $CuIn_{2n+1}S_{3n+2}$ films. Indeed, the intensity of the preferential orientations of $CuIn_{2n+1}S_{3n+2}$ thin films (112 plane for $CuInS_2$ and $CuIn_3S_5$ films and 311 plane for $CuIn_5S_8$, $CuIn_7S_{11}$ and $CuIn_{11}S_{17}$ films) increases with the the increase of the substrate temperature. This improvement of crystallinity could be explained by the fact that at higher substrate temperatures, the mobility of the condensing particles on the substrate surface is more, which favors the crystallization and the growth of large crystallites [19], similar explanation was reported by Bacaksiz et *al.* [20] who observed an improvement in the crystal structure by increasing the substrate temperature, and that can be explained in term of higher ad-atom mobility with increasing temperatures, which results in the larger grain size and enhances the crystallinity of the films. We also note that the XRD patterns of all samples do not contain extra reflections corresponding to the elements or other secondary phases, which confirms the homogeneity of the $CuIn_{2n+1}S_{3n+2}$ films.

To obtain detailed information about the structural properties, the grain size, dislocation density, strain and lattice parameters for preferential orientations were calculated using the XRD patterns of $CuIn_{2n+1}S_{3n+2}$ films. The lattice parameters a and c of $CuInS_2$ and $CuIn_3S_5$ were determined from the analysis of the XRD patterns and were estimated by using Equation (1) whereas Equation (2) was used to calculate the lattice parameter a of $CuIn_5S_8$, $CuIn_7S_{11}$ and $CuIn_{11}S_{17}$ [21].

$$\frac{1}{d^2} = \frac{h^2+k^2}{a^2} + \frac{l^2}{C^2} \qquad (1)$$

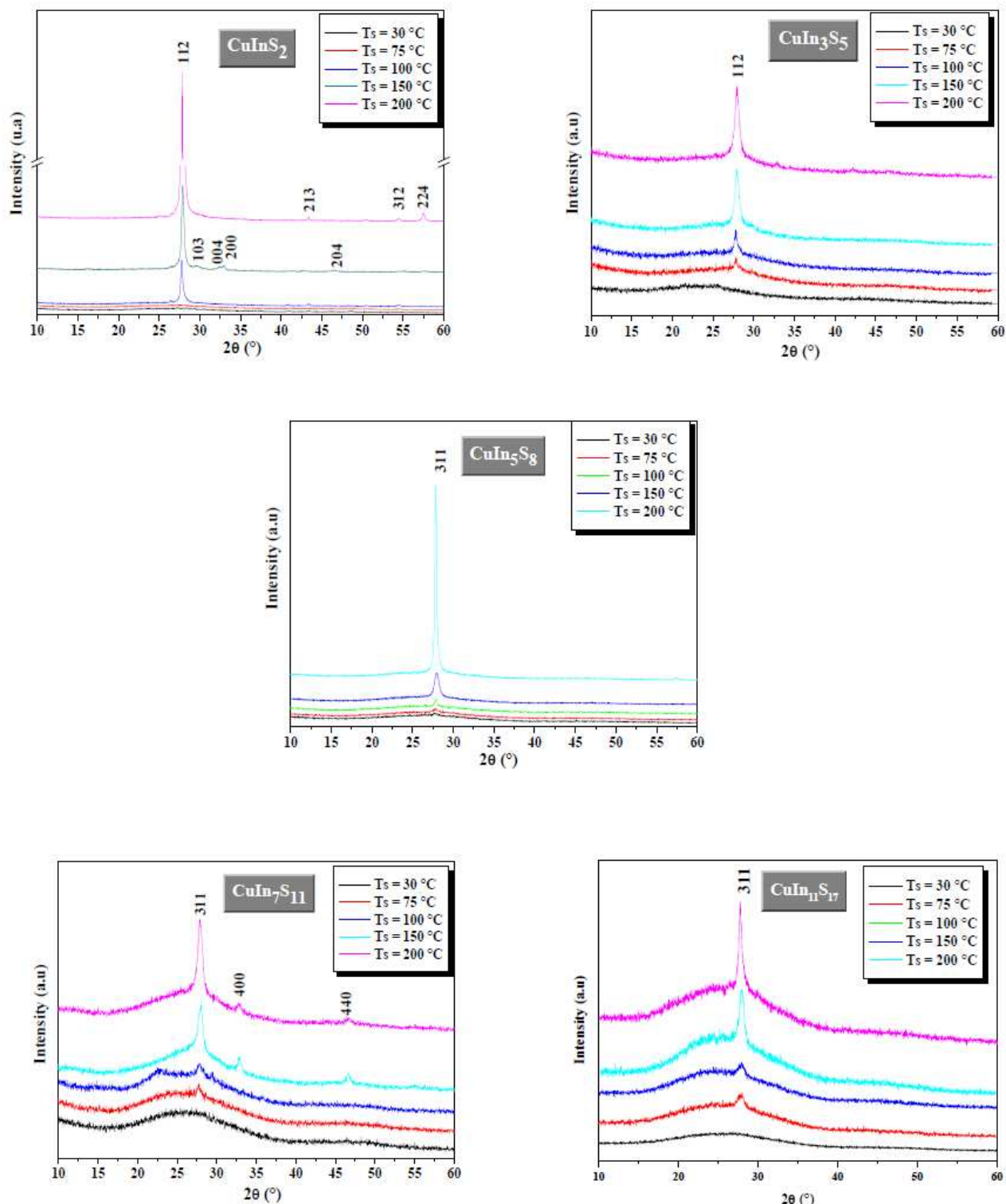$$\frac{1}{d^2} = \frac{h^2+k^2+l2}{a^2} \qquad (2)$$

Fig. 1: The X-ray diffraction patterns of $CuIn_{2n+1}S_{3n+2}$ thin films deposited at different substrate temperatures.

In these equations, h, k and l are the miller indices and d_{hkl} is the crystalline plane distance for indices (hkl) determined using Bragg's equation:

$$2d \sin \theta = \lambda \qquad (3)$$

where λ is the wavelength of the radiation, and θ is the diffraction angle. The calculated values of the lattice parameters of all samples were collected in Table **1**.

The effect of the substrate temperature on the grain size D of $CuIn_{2n+1}S_{3n+2}$ thin films was also investigated. Grain size can be simply determined using the Debye-Scherrer formula [22]:

$$D = \frac{0.9\lambda}{\beta \cos \theta} \qquad (4)$$

where λ is the wavelength of CuK_α radiation, β is the values of the full width at half maximum (FWHM) of the peak with maximum intensity (112 peak for $CuInS_2$ and $CuIn_3S_5$ films and 311 peak for $CuIn_5S_8$, $CuIn_7S_{11}$ and $CuIn_{11}S_{17}$ films) and θ is the diffraction angle of the peak. The variation of grain size with the substrate temperature is shown in Fig. **2**.
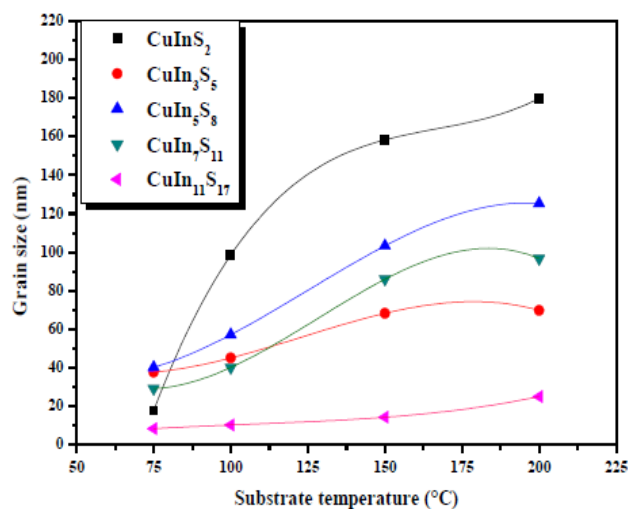
might form a joint structure in the case for which the total free energy is reduced by the formation of an interface. Thin films (thermally evaporated) which we produce are a consequence of kinetic restraints [24]. In the case for which some mobility of the ad-atoms is possible, competitive grain growth occurs [25]. In thin film growth, we can influence the kinetics by temperature. The mobility of the ad-atoms is influenced by this factor and so the mobility of grain boundaries. We also note that $CuInS_2$ films have the biggest crystallite size in comparison to those of other material films, which confirms that the $CuInS_2$ has a crystalline quality higher than those of the other compounds.

The strain in thin films originates from the difference in the thermal expansion coefficients of the deposited material and the substrate and the stoichiometric deviations which depends on the deposition conditions. The values of the lattice strain ε of $CuIn_{2n+1}S_{3n+2}$ thin films were calculated using Williamson-Hall formula [26]:

$$\varepsilon = \frac{\beta}{4 \tan \theta} \qquad (5)$$

where θ is the diffraction angle and β is the values of the full width at half maximum (FWHM) of the (112) and (311) peaks, respectively.
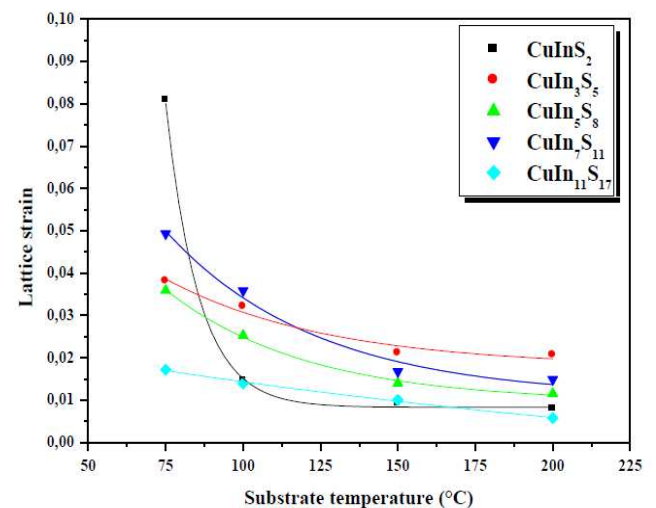

Fig. 2: Grain size of $CuIn_{2n+1}S_{3n+2}$ thin films deposited at different substrate temperatures.

Fig. 3: Lattice strain of $CuIn_{2n+1}S_{3n+2}$ thin films deposited at different substrate temperatures.

As is seen, the grain size of $CuIn_{2n+1}S_{3n+2}$ films increases with the increase of T_s. This increase could be attributed to the improvement in the mobility of surface ad-atoms and an increase in the cluster formation leading to agglomeration of small grains [23]. Indeed, thermodynamically, the film material would prefer to be compact, bounded by low index planes. The same holds for the substrate. Together, the film and the substrate

Fig. **3** shows the variation of ε with the substrate temperature, which indicated a reduction in the strain with the increase of substrate temperature. The change of D and e with T_s suggest that lower the lattice strain, higher will be the grain size. This implies that lattice strain in thin films restricts the growth of grains in films

because tensile strain is generated at the grain boundaries by shrinking the distance between adjacent grains [27]. Since grain size increases with substrate temperature, the number of grains will be decreased. This decrease may be the main agent for the decrease of the lattice average strain.

Table 1: Lattice parameters of $CuIn_{2n+1}S_{3n+2}$ (n = 0, 1, 2, 3 and 5) thin films at different substrate temperature.

|		75 °C	100 °C	150 °C	200 °C
CuInS$_2$	a (Å)	-	5.55	5.53	5.55
	c (Å)	-	11.11	11.06	11.11
CuIn$_3$S$_5$	a (Å)	5.54	5.56	5.51	5.49
	c (Å)	11.08	11.13	11.03	10.99
CuIn$_5$S$_8$	a (Å)	10.64	10.60	10.60	10.64
CuIn$_7$S$_{11}$	a (Å)	10.66	10.66	10.66	10.68
CuIn$_{11}$S$_{17}$	a (Å)	10.59	10.60	10.61	10.68

From the values of grain size *D*, we also calculated the average dislocation density of $CuIn_{2n+1}S_{3n+2}$ films elaborated at different substrate temperatures using the following formula [28]:

$$\delta = \frac{1}{D^2} \qquad (6)$$

The variation of dislocation density with substrate temperature is shown in Fig. **4**. As is seen, the dislocation density decreases by increasing the substrate temperature. δ values indicate the amount of defects in the structure. So, the decrease of δ indicates that the defects in the structure decrease and consequently, indicates the improvement of the crystallinity of $CuIn_{2n+1}S_{3n+2}$ films by increasing T_s.

5 Conclusions

$CuIn_{2n+1}S_{3n+2}$ films (with n = 0, 1, 2, 3 and 5) were prepared at different substrate temperatures (30, 75, 100, 150, 200 $^{\circ C}$ on glass substrate using the vacuum evaporation technique. The XRD spectra indicate that the $CuIn_{2n+1}S_{3n+2}$ films can be formed in different structures. Indeed, for n = 0 and 1, the films crystallize in the chalcopyrite structure with the preferential orientation along (112) plane. On the passage to n = 2, 3 and 5, $CuIn_5S_8$, $CuIn_7S_{11}$ and $CuIn_{11}S_{17}$ films crystallize in the spinel structure with the preferential orientation along (311) plane. This study shows that the crystal quality of $CuIn_{2n+1}S_{3n+2}$ films is strongly correlated with the substrate temperature. Indeed, the increase of substrate temperature allows an amorphous-to-crystalline phase transition and the improvement of the crystalinity of films.
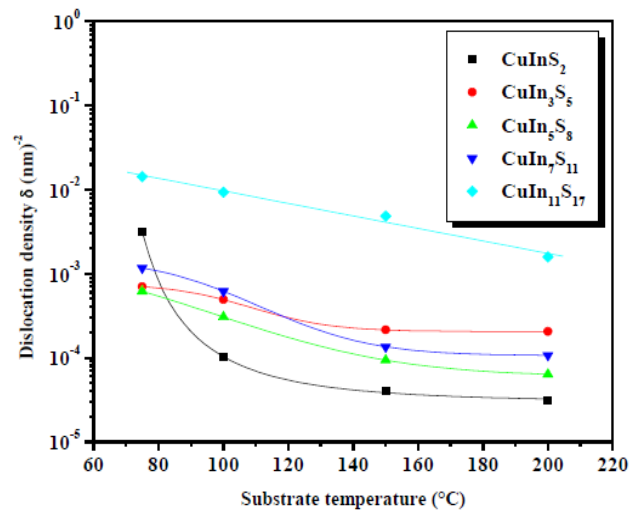
Fig. 4: Dislocation density of $CuIn_{2n+1}S_{3n+2}$ thin films deposited at different substrate temperatures.

References

[1] C. Mahendran and N. Suriyanarayanan, Physica B, **405**, 2009-2013 (2010).

[2] M. Ben. Rabeh, N. Chaglabou and M. Kanzari, Chalcogenide Letters, **6**, 83-89 (2009).

[3] C. Broussillou , M. Andrieux , M. H. Ghysel, M. Jeandin, J. S. Jaime-Ferrer, S. Bodnar and E. Morin, Solar Energy Materials & Solar Cells, **95**, 13-17 (2011).

[4] R. Klenk, J. Klaer, C. Kble, R. Mainz, S. Merdes, H. Rodriguez-Alvarez, R. Scheer and H.W. Schock, Solar Energy Materials & Solar Cells, **95**, 1441-1445 (2011).

[5] I. V. Bodnar, Inorganic Materials, **44**, 104-109 (2008).

[6] V. Yu. Rud, Yu. V. Rud, I. V. Bodnar, D. V. Gorbachev, and T. N. Ushakova, Fizika i Tekhnika Poluprovodnikov, **43**, 391-395 (2009).

[7] F. Bensebaa, C. Durand and A. Aouadou, Journal of Nanoparticle Research, **12**, 1897-1903 (2010).

[8] S. Peg, F. Cheng, J. Liang, Z. Tao and J. Chen, Journal of Alloys and Compounds, **48**, 786-791 (2009).

[9] J. Guo,W. H. Zhou, M. Li, Z. L. Hou, J. Jiao, Z. J. Zhou and S. X. Wu, Journal of Crystal Growth, **359**, 72-76 (2012).

[10] D. Li, Y. Zou and D. Yang, Journal of Luminescence, **132**, 313-317 (2012).

[11] R. R. Philip, S. Dhanya, T. N. Ashokan and B. Pradeep, Journal of Physics and Chemistry of Solids, **72**, 294-29 (2011).

[12] M. Rusu, S. Wiesner, R. Wrz, S. Lehmann, S. D. Yamigno, A. Meeder, D. F. Marrnc, M. Br, V. Koteski, H. E. Mahnke, E. Arushanov, J. Beckmann, K. Hhn, W. Fritsch, W. Bohne, P. S. Bischoff, M. Heuken, A. J. Waldau, A. Rumberg and Th. S. Niedrig, Solar Energy Materials and Solar Cells, **95**, 1555-1580 (2011).

[13] J. L. Orts, R. Dïaz, P. Herrasti, F. Rueda and E. Fats, Solar Energy Materials & Solar Cells, **91**, 621-628 (2007).

[14] M. A. Majeed Khan, S. Kumar, M, Ahamed and M. S. AlSalhi, Materials Letters, **68**, 497-500 (2012).

[15] S. Mehdaoui, N. Benslim, M. Benabdeslem, O. Aissaoui, L. Bechiri and X. Portier, Energy Procedia, **10**, 94-100 (2011).

[16] M. V. Yakushev, A. V. Mudryi, V. F. Gremenok, E. P. Zaretskaya, V. B. Zalesski, Y. Feofanov and R.W. Martin, Thin Solid Films, **451**, 133-136 (2004).

[17] Y. L. Wu, H. Y. Lin, C. Y. Sun, M. H. Yang and H. L. Hwang, Thin Solid Films, **168**, 113-122 (1989).

[18] N. Khemiri, D. Abdelkader, B. Khalfallah and M. Kanzari, Open Journal of Synthesis Theory and Applications, **2**, 33-37 (2013).

[19] K. J. Patel, M. S. Desai and C. J. Panchal, Adv. Mat. Lett., **3**, 410-414 (2012).

[20] E. Bacaksiz, S. Aksu, I. Polat, S. Yilmaz and M. Altunbas, Journal of Alloys and Compounds, **487**, 280-285 (2009).

[21] M. Ladd and R. Palmer, Structure Determination by X-ray Cristallography, Plenum Publishers, New York, (2003).

[22] S. J. Ikhmayies and R. N. A, Bitar, Applied Surface Science, **256**, 3541-3545 (2010).

[23] A. S. Reddya, H. H. Parka, G. M. Paob, S. Uthannac and P. S. Reddyc, Journal of Alloys and Compounds, **474**, 401-405 (2009).

[24] G. C. A. M. Janssen, Thin Solid Films, **51**, 6654-6664 (2007).

[25] M. Pellicone, T. Karabacak and T. M. Lu, Phys. Rev. Lett., **96**, 146105-146110 (2006).

[26] A. R. Shetty, A. Karimi and M. Cantoni, Thin Solid Films, **519**, 4262-4270 (2011).

[27] S. C. Seel, C. V. Thompson, S. J. Hearne and J. A. Floro, J. Appl. Phys., **88**, 7079-7083 (2000).

[28] S. Kose, F. Atay, V. Bilgin and I. Akyuz, Materials Chemistry and Physics, **111**, 351-358 (2008).